Quasiclassical trajectory study of $O(^1D)+N_2O \rightarrow NO+NO$: Classification of reaction paths and vibrational distribution

Shinnosuke Kawai,[a] Yo Fujimura,[b] and Okitsugu Kajimoto
Department of Chemistry, Graduate School of Science, Kyoto University, Kitashirakawa-Oiwakecho, Sakyo-ku, Kyoto 606-8502, Japan

Takefumi Yamashita
Department of Basic Science, Graduate School of Arts and Sciences, University of Tokyo, Komaba, Tokyo 153-8902, Japan

(Received 9 December 2005; accepted 6 March 2006; published online 11 May 2006)

Quasiclassical trajectory calculations for the planar reaction of $O(^1D)+N_2O \rightarrow NO+NO$ are performed on a newly constructed *ab initio* potential energy surface. In spite of the reduced dimension approximation, the agreement between the computational and experimental results is largely satisfactory, especially on the similar amount of excitation of the two kinds of NO products found by Akagi *et al.* [J. Chem. Phys. **111**, 115 (1999)]. Analyzing the initial condition dependence of the trajectories, we find that the trajectories of this reaction can be classified into four reaction paths, which correspond to respective areas in the space of initial condition. In one of the four paths, a long-lived stable complex is formed in the course of reaction, whereas the other three paths have direct mechanism. Contradictory to conventional understanding of the chemical reaction dynamics, the direct paths show more efficient energy exchange between the NO stretching modes than that with a long-lived intermediate. This indicates that the vibrational mode coupling along the short-lived paths is considerably stronger than expected. © *2006 American Institute of Physics*.
[DOI: 10.1063/1.2191041]

I. INTRODUCTION

Nascent state distribution of reaction products is the major experimental information on reaction dynamics. Until today it has been generally believed[1] that the product state distribution is closely related to the stability of the reaction intermediate, that is, the depth of the well on the potential energy surface (PES) of the system. If the PES possesses a deep well, the system is expected to be trapped in it for a sufficiently long period which enables energy randomization, resulting in a statistical distribution of the products. On the other hand, if there is no significant well on the PES, the lifetime of the intermediate is likely to be short and the energy is distributed in only a part of the rovibrational modes of the products.

However, contradictory experimental results[2,3] were found for the reaction of $O(^1D)$ with N_2O:

$$O(^1D) + N_2O \rightarrow NO + NO, \quad \Delta H_f^o(0) = -341 \text{ kJ/mol}, \tag{1}$$

$$O(^1D) + N_2O \rightarrow N_2 + O_2, \quad \Delta H_f^o(0) = -520 \text{ kJ/mol}. \tag{2}$$

Many experimental studies[2–11] have been done by measuring product state distributions and vector properties for channel (1). The two NO products should be distinguished from dynamical viewpoint. Hereafter we use prime symbols for this purpose and express the reaction as follows:

$$O(^1D) + NN'O' \rightarrow NO + N'O'. \tag{3}$$

The newly formed NO originating from $O(^1D)$ is called a "new" NO and the $N'O'$ which already exists in the reactant N_2O is called an "old" NO. Agagi *et al.*[2,3] distinguished these two kinds of NO by using isotopically labeled $^{18}O(^1D)$, and measured the individual vibrational state distributions for $v' \leqslant 17$. The sum of the distribution of the new and old NO products decreased monotonically as the vibrational quantum number increased and was very close to the statistical distribution up to $v' \approx 10$ and became smaller than the statistical one for higher v'. The statistical nature of the vibrational distribution was further confirmed by the measurement with Fourier transform infrared spectrometer.[7,10] Furthermore, although the vibrational distribution of the new NO is more excited than that of the old NO, the populations of both types of the products in each vibrational level are not significantly different.[2,3] This nearly equal energy partitioning between the two kinds of NO is surprising because neither experiments[12,13] nor calculations[14–18] have found any deeper well for this reaction than the *cis*-planar NO dimer, whose binding energy of 8.3 kJ/mol (Ref. 13) relative to NO+NO is very small compared with the exothermicity of 341 kJ/mol. This result forms a sharp contrast to the $O(^1D)+H_2O$ reaction, whose two types of OH products show entirely different vibrational

[a]Present address: Laboratoire de Chimie Théorique, Faculté des Sciences, Université de Sherbrooke, Sherbrooke, Québec, Canada J1K 2R1. Electronic mail: S.Kawai@USherbrooke.ca
[b]Present address: The Center for Basic Education and Integrated Learning, Kanagawa Institute of Technology, 1030 Shimo-Ogino, Atsugi, Kanagawa 243-0292, Japan. Electronic mail: fujimura@gen.kanagawa-it.ac.jp

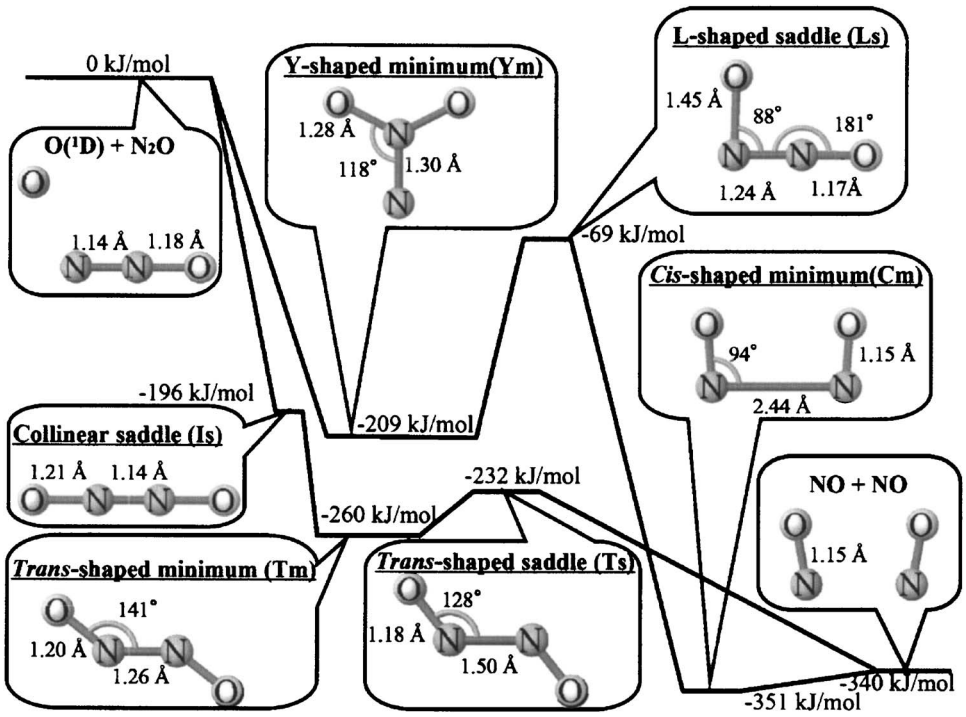

FIG. 1. Schematic representation of the stationary points and energy profile of our new PES. Their names and geometries are shown in the insets.

distributions[19,20] although the reaction is considered to proceed with stable H_2O_2 intermediate.[21]

In theoretical works, González *et al.*[15] have performed high-level *ab initio* calculations at the stationary points for the $O(^1D)+N_2O$ reaction and obtained the rate constants using transition state theory and quasiclassical trajectory (QCT) calculation on a fitted pseudotriatomic London-Eyring-Polanyi-Sato surface. Although they found relatively good agreement with the experimental results in the rate constants and branching ratios, their *ab initio* calculation was limited to the neighborhoods of the stationary points and was not adequate for dynamical studies on global PES. Takayanagi and co-workers[16–18] constructed a global PES by calculating *ab initio* energies at about 10 000 grid points of planar configuration and fitted them to an analytical form. Using this $^1A'$ ground surface, they performed QCT calculation with zero impact parameter[18] and quantum calculations.[17,22] They found qualitative agreement with the experimental results on vibrational distribution and branching ratio. They also pointed out the existence of "scrambling" process:

$$O(^1D) + NN'O' \rightarrow NO' + N'O, \tag{4}$$

whose contribution was smaller than that of the normal NO channel (3) but not negligible. Recently, the authors used this PES to calculate the product rotational distribution and compared the results with the experiment.[11] To elucidate the dynamics, we carried out two types of calculations, one of which utilized only the exit region of the PES. Although we had relatively good agreement with the experiment by this type of calculation, the calculation using the full PES showed less satisfactory results.

In this paper, our purpose is to clarify the detailed reaction mechanism based on the QCT analyses. In Sec. II, we construct a new global PES function and characterize it with the minima and saddles. In Sec. III, we perform the QCT calculations in order to investigate the dynamical features. We show that the reaction dynamics are clearly dependent upon the initial condition and the reactive trajectories can be classified into four paths. One of the paths is found to have a long lifetime, being trapped in a Y-shaped well, whereas the other paths exhibit a short lifetime. Contrary to the general notion, we find that the old NO vibration is highly excited along the short-lifetime paths rather than the long-lifetime one. Finally, we conclude in Sec. IV.

II. POTENTIAL ENERGY SURFACE

To construct the global PES, we performed *ab initio* calculations for about 10 000 geometries in planar configuration. Here, we employed CASPT2$(10_e,8_o)$/cc-pVDZ, which is the same level as that by Takayanagi and co-workers.[16–18] We note that they showed that the calculations of this level provided reasonable results.[18,22] These calculated energies were fitted to an analytical form (the details about constructing PES function are given as supplemental materials).[23] The root mean square of the fitting error is 4.096 kJ/mol and the maximum value of the error is 19.96 kJ/mol. In this paper, we used the MOLPRO program for all the *ab initio* calculations.[24]

The energy profile with stationary points of the new PES are schematically shown in Fig. 1. The PES has several minima and saddle points rather than a single shallow well. The collinear saddle (Is), Y-shaped minimum (Ym), and L-shaped saddle (Ls) are newly found in this work. The

TABLE I. Geometies and energies of stationary points. Results of higher-level calculation in Ref. 15 are shown in parentheses, when available. The available experimental data are shown in brackets.

Stationary point	R_{NN} (Å)	R_{NO} (Å)	∠NNO (deg)	Dihedral (deg)	Energy (kJ mol^{-1})
Is	1.1409	1.2120, 1.2120	180.0, 180.0	180	−196
Tm	1.2597	1.1971, 1.1971	141.4, 141.4	180	−260
	(1.2700)[a]	(1.2099, 1.2099)[a]	(137.7, 137.7)[a]	(180)[a]	(−277)[ab]
					(−174)[ac]
Ts	1.5015	1.1814, 1.1814	127.9, 127.9	180	−232
	(1.4578)[d]	(1.1892, 1.1892)[d]	(129.5, 129.5)[d]	(180)[d]	(−258)[bd]
					(−167)[cd]
Ym	1.2977	2.2056, 1.2817	31.0, 117.5	180	−209
Ls	1.2407	1.4540, 1.1679	87.7, 179.3	180	−69
Cm	2.4376	1.1527, 1.1527	94.3, 94.3	0	−351
	(3.0623)[e]	(1.1603, 1.1603)[e]	(90.8, 90.8)[e]	(0)[e]	(−345)[be]
					(−329)[ce]
	[2.2630][f]	[1.1515, 1.1515][f]	[97.2, 97.2][f]	[0][f]	[−353][g]

[a]MIN *B*1 of Ref. 15.
[b]CASPT2//CASSCF(18,14) level calculation of Ref. 15.
[c]CASSCF(18,14) level calculation of Ref. 15.
[d]TS *B*1 of Ref. 15.
[e]MIN *D*1 of Ref. 15.
[f]Experimental data taken from Ref. 27.
[g]Experimental data derived from Refs. 13 and 28.

imaginary frequency mode at Is corresponds to the isomerization between two *trans*-shaped minima (Tm):

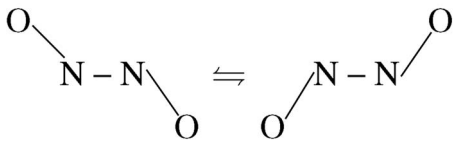

(5)

These two configurations are energetically equivalent and therefore only one of them is shown in Fig. 1, but they must be distinguished in the planar configuration space. As will be shown later in Sec. III C, trajectories go downhill along a bath mode direction of Is and then fall into one of the *trans* minima following the reactive (imaginary) mode of Is. The Ym plays important roles, as seen in Sec. III. Particularly, the scrambling process occurs in the Ym well, which can trap the trajectories for a long time. From the additional *ab initio* calculations, we checked that the Ym has the real frequency of the out-of-plane vibration mode. Thus, we can consider that the Y-shaped minimum exists in the real $O(^1D)+N_2O$ system. This structure can be also expected by the analogy with NO_3 molecule, whose equilibrium geometry is D_{3h}.[25] Although the electronic wave functions of both can be described by a single Slater determinant, Eisfeld and Morokuma[25] revealed that the insufficient dynamic and static correlations lead to the symmetry breaking problem for NO_3. The recent density functional theory (DFT) calculation of N_2O_2 also indicated that C_{2v} symmetry of the Y-shaped structure is broken.[26] This fact also shows that DFT level calculation is not appropriate for this system as emphasized by González *et al.*[15]

Table I shows geometries and energies of stationary points found in our new PES with those found by González *et al.*[15] and experimental data.[13,27,28] At these points, we also calculate the vibrational frequencies of the planar normal modes, which are summarized in Table II. Here we adopt 14 and 16 amu for the masses of nitrogen and oxygen, respectively, in order to compare them with the results of the former works.[15,28] The geometrical parameters and normal mode frequencies of reactant $[O(^1D)+N_2O]$ and products ($NO+NO$ and O_2+N_2) are the same as those of the PES of Takayanagi and Akagi[18] and agree with those of the experiments. The stationary points listed in Tables I and II have large effects on dynamics, as will be explained in Secs. III B and III C. González *et al.* found more stationary points through larger CASSCF(18,14) calculations,[15] although we consider that their contribution to the dynamics is minor to reproduce the product vibrational distribution. The *trans*-shaped minimum (Tm) and saddle (Ts) points can be considered to correspond to "MIN *B*1" and "TS *B*1" of González *et al.*, respectively. Our geometries for these points are in good agreement with those of González *et al.*, while the energies are slightly lower. The normal mode frequencies are in qualitative agreement, as seen in Table II. The *cis*-shaped minimum (Cm) corresponds to "MIN *D*1" of González *et al.* and experimentally found NO dimer.[12,13,27,28] For this minimum point, we have obtained better agreement with the experiment than with González *et al.* In particular, the R_{NN} for our PES is considerably (by 0.63 Å) closer to the experimental one than to that by González *et al.*

III. RESULTS AND DISCUSSIONS

In QCT calculations, the classical equations of motion for the $O(^1D)+N_2O$ collision were numerically integrated by fourth-order Runge-Kutta method with variable time step.[29] We confirmed the total energy conservation better than 10 cm^{-1}. Since the *ab initio* PES is only available for planar configurations, the dynamics calculations were confined in two-dimensional collision plane. However, we can consider

TABLE II. Harmonic vibrational frequencies (in cm^{-1}) of in-plane normal modes at the stationary points. The symmetries of the vibrational modes are given in parentheses. Results of higher-level calculation in Ref. 15 are shown in parentheses, when available. The available experimental data are shown in brackets.

Stationary point	ω_1	ω_2	ω_3	ω_4	ω_5
Is	688.6*i* (π_g)	2658.0 (σ_g^+)	1258.2 (σ_u^+)	906.4 (σ_g^+)	316.2 (π_u)
Tm	2080.7 (a_g)	1486.9 (b_u)	858.1 (a_g)	622.2 (a_g)	485.3 (b_u)
	(1672.4)[a]	(1520.2)[a]	(810.2)[a]	(496.6)[a]	(401.8)[a]
Ts	750.9*i* (a_g)	1611.2 (ag)	1538.1 (b_u)	442.8 (a_g)	415.8 (b_u)
	(561.4*i*)[b]	(1610.5)[b]	(1604.7)[b]	(398.4)[b]	(611.1)[b]
Ym	1907.7 (a_1)	1465.2 (b_2)	1324.9 (a_1)	692.6 (a_1)	254.1 (b_2)
Ls	661.0*i* (a')	2223.7 (a')	1195.4 (a')	689.0 (a')	368.8 (a')
Cm	1877.5 (a_1)	1862.8 (b_1)	460.7 (b_1)	214.3 (a_1)	156.1 (a_1)
	(1890.5)[c]	(1886.2)[c]	(113.2)[c]	(85.0)[c]	(31.2)[c]
	[1863.4][d]	[1776.3][d]	[242.9][d]	[299.3][d]	[175.4][d]

[a]MIN *B*1 of Ref. 15.
[b]TS *B*1 of Ref. 15.
[c]MIN *D*1 of Ref. 15.
[d]Experimental data taken from Ref. 28.

that this planar dynamics contains the essential features of this reaction because of the good agreement with the experimental results as we will see in Sec. III A. To compare our results with the experiments of Akagi *et al.*,[2,3] we employed the nuclear masses of $^{18}O+{}^{14}N^{14}N^{16}O$ and the collision energy was fixed to 20.9 kJ/mol, which corresponds to the mean value under their experimental condition.

A. Product vibrational distribution

Figure 2(a) shows the calculated product vibrational distributions for $N^{18}O$ (new NO) and $N^{16}O$ (old NO) with the experimental ones of Akagi *et al.*[3] and Hancock and Havend.[10] The results of Hancock and Haverd which do not distinguish the two NO's, appear mainly in the region between the two distributions of Akagi *et al.* In QCT calculations, we sampled about 200 000 trajectories whose initial conditions were chosen according to the classical Boltzmann distribution of N_2O rotation at 300 K and the zero-point vibrational energy of the present PES. As mentioned above, there are two channels to NO+NO: the normal product channel (3) and the scrambled channel (4). The experiment of Akagi *et al.*[3] distinguished the two O atoms by using isotopically labeled $^{18}O(^1D)$ but not the N atoms. Thus, in order to make a comparison with their experiment, we show in Fig. 2(a) the sum of the population of NO and N′O by downward open triangles, and that of N′O′ and NO′ by upward open triangles. The former corresponds to the new NO of Ref. 3 and the latter to the old NO. The computational and experimental distributions agree well on their qualitative features in that both distributions decrease monotonically as product vibrational energy increases and the difference between the vibrational distributions of $N^{18}O$ and $N^{16}O$ is small, although the QCT underestimates vibrational excitation slightly. Taking into account the fact that our QCT calculations do not include the out-of-plane motion, the agreement between the measured and calculated results is so good that we can consider that our planar model includes the essential features of this reaction. We also calculated the product vibrational distributions for each channel. The results are shown in Fig. 2(b). The closed triangles show the vibrational distribution of the normal product channel (3), with downward triangles depicting new NO (NO) and upward ones old NO (N′O′). The gray triangles show the distribution of the scrambled channel (4), with downward triangles depicting N′O and upward ones NO′. The product vibrational distributions for the normal product channel are very similar to the total ones, while the contribution of the scrambled channel is minor, but not negligible.

For further investigation of the dynamics, we first examined the effect of initial rovibrational motion of the reactant N_2O by performing additional QCT calculations where N_2O is initially fixed to its equilibrium configuration with zero rovibrational momenta. Figure 2(c) shows the resulting product vibrational distributions. Comparing Fig. 2(c) with 2(b), we can see that the vibrational excitation is diminished probably due to the smaller amount of total energy. However, the qualitative features like the similarity between the two NO's are well conserved. Therefore we can consider that the effect of initial rovibrational motion is minor and most of the important dynamical features of this system are still contained in the dynamics with the zero rovibrational energy of initial N_2O. The reason of this is likely to be the large exothermicity of this reaction. The sum of zero-point energy and 300 K rotational energy of N_2O amounts to ca. 2000 cm^{-1}, which is less than 10% of the exothermicity and therefore is not likely to affect the dynamics. This result allows us to investigate the dynamics with fixed initial condition of N_2O.

This simplification enables us to easily elucidate the initial condition dependence of the dynamics, because now we can specify the initial condition with only two parameters: impact parameter b and initial orientation angle ψ of N_2O as defined in Fig. 3. In Sec. III B we will examine the reaction dynamics by analyzing the dependence on these two parameters.

B. Initial condition dependence of dynamics

We have seen in Sec. III A that the initial condition of this reaction system can be specified with only two parameters. Here we analyze the dynamics by plotting various properties of trajectories on two-dimensional space of initial

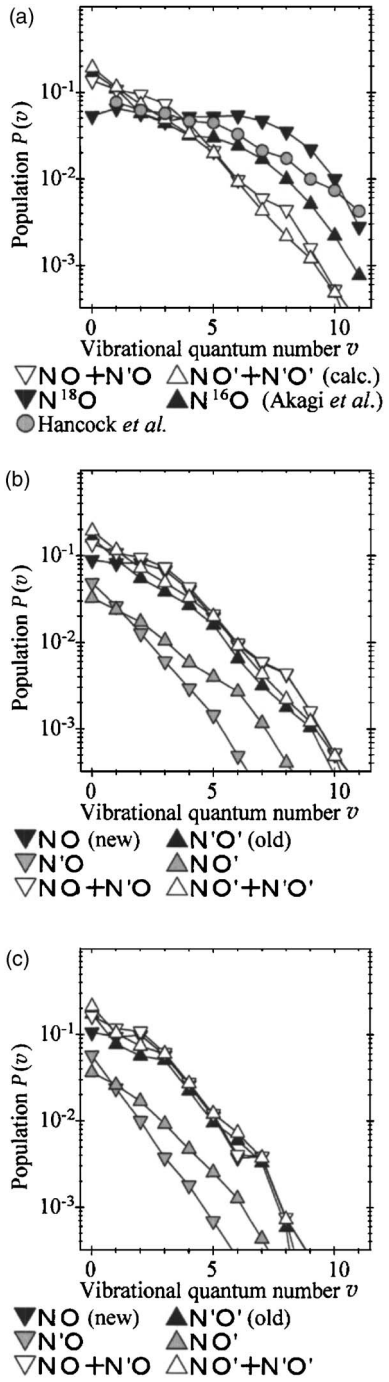

FIG. 2. Vibrational distribution of NO produced from $O(^1D)+N_2O$ obtained from experiment and calculation. (a) Comparison of the QCT and experimental results. Open triangles depict the results of QCT calculation. Closed triangles show experimental results of Akagi *et al.* (Ref. 3). Gray circles show the results of Hancock and Haverd (Ref. 10). (b) Results of QCT calculation of this work. Initial rovibrational state of N_2O is sampled by thermal rotational distribution and zero-point vibrational energy. Closed triangles denote the vibrational distribution of $O(^1D)+NN'O' \rightarrow NO+N'O'$ reaction channel. Gray triangles show those of $N'O+NO'$ channel. Sum of these two channels is shown by open triangles. (c) Same as (b) except that N_2O is initially fixed to its equilibrium geometry with zero rovibrational energy.

conditions parametrized by b and ψ. First, the final product channels of trajectories are plotted in Fig. 4. For each combination of (b,ψ), the final product channel of the trajectories starting with that initial condition is shown by colors. White

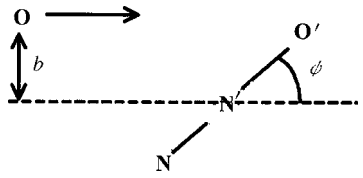

FIG. 3. Definitions of the impact parameter b and the initial orientation angle ψ of N_2O.

region means that no reaction occurs for that (b,ψ). The initial conditions leading to O_2+N_2 channel are localized in the region with relatively large $|\psi|$, which corresponds to the approach of $O(^1D)$ to the O-end side of N_2O. For those leading to NO products, we need to distinguish the normal $(NO+N'O')$ and the scrambled $(NO'+N'O)$ channels. The former is shown by light gray and the latter by black in Fig. 4. In the figure, some regions are covered only by gray color $(NO+N'O')$, while other regions have a mosaic pattern with gray and black $(NO'+N'O)$. In the other channels, atom exchange reactions, such as $NN'O+O'$, are minor and almost imperceptible in the figure. Although some parts of the initial condition space have mosaic pattern for the final channel, the mosaic pattern is localized in certain regions. The initial conditions leading to O_2+N_2 and $NO+N'O'$ channels are also localized. Thus we can state that this system has a kind of regularity in that the initial condition space may be divided into some regions which have different dynamical properties.

To obtain further insight into the dynamics, we calculated the following two quantities for each trajectory. One is the lifetime of the reaction intermediate. To estimate the lifetime, we needed to define the regions of "reactant," "product," and "reaction intermediate." By using the nuclear distances, geometries with R_{ON}, $R_{ON'}$, $R_{OO'}>2$ Å were regarded as reactant $(O+NN'O')$, those with $R_{NO'}$, $R_{ON'}$, $R_{NN'}$, $R_{OO'}>2.5$ Å as normal $NO+N'O'$ product, those with R_{NO}, $R_{O'N'}$, $R_{NN'}$, $R_{OO'}>2.5$ Å as scrambled $NO'+N'O$ product, and those with R_{ON}, $R_{O'N'}$, $R_{O'N}$, $R_{ON'}>2$ Å as O_2+N_2 product. These values were determined by inspecting the PES and specifying the region where the interaction of the two molecules is negligible. If the system is in none of these four regions, it was regarded as intermediate, and its lifetime τ is defined as the length of time during

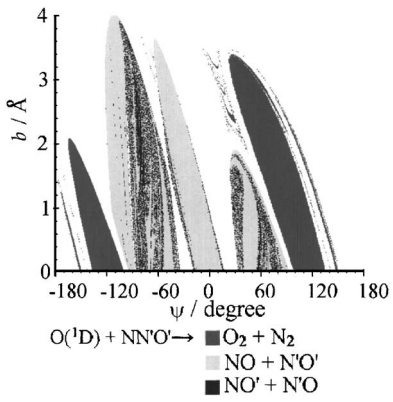

FIG. 4. Final product channel of the reaction is plotted against the initial conditions b and ψ (see Fig. 3 for definition).

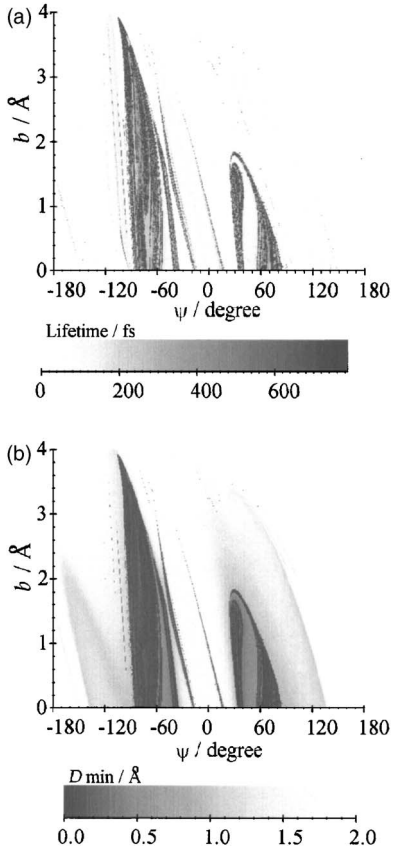

FIG. 5. (a) The lifetimes of the reaction intermediate are plotted against the initial condition. Light (dark) colors denote short (long) lifetime. (b) Value of the minimum distance $D_{\min}(\mathrm{Ym})$ from the Y-shaped minimum point is plotted against the initial condition. Light (dark) colors denote larger (smaller) values.

which the system has intermediate geometry. The lifetime τ thus defined can be interpreted as the "time delay" between the beginning of the interaction (entrance into the intermediate region) and the formation of the product (exit from the intermediate region). Martínez *et al.*[30] called a similar quantity "collision time," although they defined the intermediate region by using center-of-mass distances, not nuclear distances. With all this ambiguity of terminology, we will use the word "lifetime" for this quantity τ in all that follows, because we regard the word suitable for describing such concepts as long-lived intermediate, etc. Figure 5(a) shows the initial condition dependence of the lifetime τ. In this figure we notice that the region with large τ value, which is shown in dark colors, and that with small value, which is shown by light colors, are clearly divided in the b-ψ plane.

The other quantity is an abstract "distance" from Ym, which is meant to estimate how close the system is to Ym. We define the abstract distance $D_{\min}(\mathrm{Ym})$ as

$$D_{\min}(\mathrm{Ym}) \overset{\mathrm{def}}{=} \min_{\text{one trajectory}} \left[\frac{1}{2} \sum_{i \neq j} (R_{ij} - R_{ij}^{0})^2 \right]^{1/2}, \tag{6}$$

where i and j run over N, O, N′, and O′. R_{ij} and R_{ij}^{0} are the ij distances for the geometries of the reacting system and

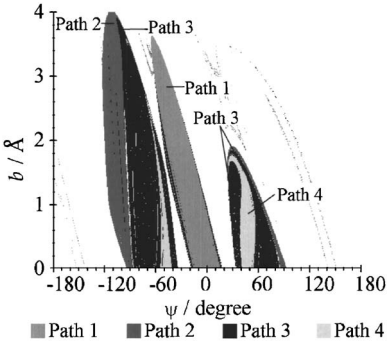

FIG. 6. Classification of the reactive trajectories. The regions of the initial conditions belonging to paths 1, 2, 3, and 4 are painted with the indicated colors.

Ym, respectively. The operator "$\min_{\text{one trajectory}}$" means searching the minimum value along one trajectory. Figure 5(b) shows the initial condition dependence of $D_{\min}(\mathrm{Ym})$. In this figure again, we can see clear distinction of the region with large $D_{\min}(\mathrm{Ym})$ value (light colors) and that with small value (dark colors).

C. Classification of trajectories and analysis of dynamics

The peculiar dependence on the initial condition shown in Sec. III B implies that there are several classes of trajectories which have different reaction mechanisms. Thus we suggest here the following classification of the trajectories leading to NO products. By using ψ, $D_{\min}(\mathrm{Ym})$, and τ introduced above and referring to Fig. 5, we have set up four groups with the definitions listed below:

$$\begin{aligned}
&D_{\min}(\mathrm{Ym}) > 0.8\ \text{Å}, \quad -80^\circ < \psi < 20^\circ \quad \text{(path 1)},\\
&D_{\min}(\mathrm{Ym}) > 0.8\ \text{Å}, \quad \psi < -80^\circ \ \text{or}\ \psi > 20^\circ \quad \text{(path 2)},\\
&D_{\min}(\mathrm{Ym}) < 0.8\ \text{Å}, \quad \tau > 160\ \text{fs} \quad \text{(path 3)},\\
&D_{\min}(\mathrm{Ym}) < 0.8\ \text{Å}, \quad \tau < 160\ \text{fs} \quad \text{(path 4)}.
\end{aligned} \tag{7}$$

Distribution of these paths is shown in Fig. 6, where the colors indicate which path the initial condition belongs to. As can be predicted from the plots of $D_{\min}(\mathrm{Ym})$ and τ, there is a clear distinction of these paths without any mosaic pattern. Trajectories of paths 3 and 4 come close to the Y-shaped minimum point while those of paths 1 and 2 do not. This distinction is well justified because we have found (though not shown here) that there is a clear gap in the distribution of $D_{\min}(\mathrm{Ym})$. The distinction of paths 1 and 2 can also be clearly seen in Fig. 6, because ψ for these paths are well separated from each other. On the contrary, the distinction of paths 3 and 4 might be artificial, since the distribution of the lifetime has no gap at $\tau = 160$ fs. Both of these paths go through the Y-shaped well and the areas of path 4 are surrounded by those of path 3 in the initial condition space.

However, this distinction is meaningful when considering whether scrambling process occurs or not. Thus, this short-lifetime component yields only normal product channel (NO+N′O′) as can be seen in Fig. 4.

TABLE III. Contribution, mean vibrational energies, and lifetime of each path.

	Path 1	Path 2	Path 3	Path 4	Total	
Contribution (%)	24	23	43	10	100	
$\langle E_{vib}\rangle$ (cm^{-1})						
NO	4600	2900	3200	4300	3600	3200 (7400[a])
N′O	···	···	1500	···	1500	
N′O′	6400	2100	1400	900	3000	3000 (3800[a])
NO′	···	···	3000	···	3000	
$\langle\tau\rangle$ (fs)	80	140	1100	100		

[a]Calculated from experimental data of Ref. 3.

In Table III, we show the contributions, mean vibrational energies of the products, and lifetimes of these paths separately. Path 3 has the largest contribution of 43%, which is four times as large as the contribution of path 4. The contributions of paths 1 and 2 are about 20%, respectively. Then, all four paths have non-negligible amount of contribution to the reaction. In what follows, we describe these paths in more detail.

1. Path 1: Direct mechanism through collinear approach to trans minimum

As can be seen from definition (7), path 1 does not approach the Y-shaped minimum and has initial orientation of almost collinear O–N–N′–O′ structure. By observing the trajectories of path 1, we have found that they have collinear approach of $O(^1D)$ to NN′O′ and then go to the *trans*-type structures associated with Tm (see also Fig. 1).

In Table III, we can see that the mean lifetime of this path is as short as 80 fs. This means that the *trans*-shaped intermediate has a short lifetime probably because of the small height of the *trans*-shaped saddle. Thus, reaction of path 1 proceeds through almost "direct" mechanism.

To investigate the contribution of this path to the vibrational distribution, we have separately calculated the vibrational distribution of only path 1. A considerable excitation of the old NO is observed in the result shown in Table III. This indicates that large amount of energy flow from the new NO to the old NO has occurred in spite of the short lifetime. This result is contradictory to the conventional understanding of the reaction dynamics and it is implied that there is a need to consider strong coupling among the vibrational modes within ONNO intermediate, especially between the two stretching vibrations of NO bonds.

2. Path 2: Direct mechanism through bent approach to trans minimum

Trajectories of path 2 as well as those of path 1 do not approach the Y-shaped minimum. The difference from path 1 is the direction of approach, as can be implied from Fig. 6. By observing the trajectories, we have found that the O atom approaches the N end of the NN′O′ through bent geometry. The system then takes an L-shaped structure and bending motions are excited, causing *cis-trans* isomerization. The intermediate dissociates immediately to the products, as we have seen for path 1.

The lifetime for path 2 is a little longer than that for path 1, but is still short. Thus, we can conclude that path 2 is also direct. In the vibrational distribution, the old NO is considerably excited, though the amount of excitation is a little less than that of path 1 (see Table III). Therefore, path 2 has strong vibrational coupling in the intermediate stage of this reaction, but the coupling in the bent structure is slightly weaker than that in the collinear one.

3. Path 3: Complex mechanism trapped in Y-shaped minimum

As can be seen from definition (7), the trajectories of path 3 form a long-lived Y-shaped complex. Table III shows that the intermediate has a long lifetime extending to picosecond order. This long lifetime is probably due to the large barrier height at the L-shaped saddle point relative to the Y-shaped minimum. In the geometry of the Y-shaped minimum shown in Fig. 1, the two O atoms are equivalent except for their masses. Therefore, once the system is equilibrated after being trapped in the well, it has almost equal probability to dissociate into both of NO+N′O′ and N′O+NO′ channels, because the isotopic labeling is not likely to affect the dynamics considerably. After passing over the barrier at the L-shaped saddle point, the system dissociates immediately to the product.

Table III also shows mean product vibrational energies of path 3. In each of the two channels, the two NO products have quite different vibrational energies. To be more precise, NO has larger vibrational energy than N′O′ in the normal product (NO+N′O′) channel, and NO′ has larger energy than N′O in the scrambled (NO′+N′O) channel. In both channels, the product containing the N atom has larger vibrational energy than that containing the N′ atom. It should also be noted that the vibrational distributions of N-containing products (NO and NO′) are very close, and those of N′-containing products (N′O′ and N′O) are also close. For the total distributions of $N^{18}O$ and $N^{16}O$, the difference between N-containing products and N′-containing products are canceled out through summing up the distributions of NO and N′O, and those of N′O′ and NO′.

The difference in the vibrational distribution of the two NO molecules produced in the same product channel in spite of the long lifetime can be understood by noting the high barrier at the L-shaped saddle. This saddle point is 69 kJ/mol below the reactant, and this amount of energy is likely to be equilibrated after a long lifetime in the Y-shaped reaction intermediate. However, almost 80% of the total exothermicity is released *after* the system surmounts the barrier, Ls. The system spends only a short time in the exit region before dissociating to the product, and therefore the exothermicity released in the exit region of the PES has no reason to be equilibrated. At the L-shaped saddle, the NO (or NO′) bond length is longer than the equilibrium distance (1.15 Å) of isolated NO molecule, while the N′O′ (or N′O) bond has almost the same length as isolated NO. Therefore, the product molecule containing the N atom is likely to be vibrationally excited more than that containing the N′ atom. This explains the trend seen in Table III.

4. Path 4: Direct mechanism through Y-shaped minimum

The trajectories of path 4 go through similar regions to those of path 3, that is, they go through the Y-shaped well, surmount the L-shaped saddle, and then dissociate to the products. The marked difference from path 3 is its short lifetime, which can be seen from definition (7) and Table III. In spite of the large depth of the Y-shaped well, the system immediately reaches the L-shaped saddle point, after the O atom bounces back at the N′ atom. This path yields only normal product (NO+N′O′) and the resulting vibrational energy (Table III) shows the largest difference between the two NO products in the four paths.

It is an interesting case where a deep well does not always ensure a long lifetime, nor yet energy randomization. A similar situation was also found in $O(^1D)+HCl$ reaction.[30] Finally, we should also note that this short-lifetime component of the Y-shaped path is localized in the initial condition space [see Figs. 5(a) and 6]. This implies that some sort of regular behavior appears in spite of the high energy.

D. Efficient energy exchange in the direct paths

In Sec. III A, we showed that our planar dynamics on the new PES reproduces the experimental results qualitatively. The QCT analyses showed that the trajectories of this reaction can be classified into four paths, which we named paths 1, 2, 3, and 4. The largest contribution comes from path 3, in which the trajectories are trapped for a long time in the Y-shaped well. However, paths 1 and 2, which have short lifetimes, are not negligible. In these paths, the N′O′ vibration is excited more largely than that in path 3, although the trajectories have short lifetimes (see Table III). In order to characterize the energy distribution more qualitatively, we refer here to the ratio of the vibrational energies of the two NO products. In path 3, NO′ has 2.0 times larger energy than N′O in the scrambled channel (N′O+NO′), and NO has 2.3 times larger vibrational energy than N′O′ in the normal product (NO+N′O′) channel. For paths 1 and 2, which only form NO+N′O′ channel, the ratio takes much lower values of 0.7 and 1.4, respectively. This means that paths 1 and 2 have larger excitation of the old NO in spite of their direct mechanisms.

One possible reason for the excitation of the old NO in these direct paths is the change of the equilibrium nuclear distance along the reaction path. If the N′O′ bond length changes largely along the reaction path, the force is exerted in the direction of N′O′ bond during the reaction, resulting in excitation of N′O′ vibration. From Fig. 1, we can see that the equilibrium length of N′O′ changes slightly in going through the reactants, *trans*-type geometries (Tm and Ts), and the products. However, we consider that it does not fully explain the similar amount of excitation of NO and N′O′, because the change of the N′O′ bond length is rather small compared with that of the new NO. Therefore, we must consider the coupled motion of the NO and N′O′ stretching modes, rather than independent excitations of these two which accidentally have the same amount.

There are two possible scenarios for the coupled motion of the two NO stretching modes. The first one is that fully chaotic motion is developed in a short period and results in near-statistical distribution of the product. The second possibility is that the motion is a regular type, but this regular motion has similar projections onto both of the two NO vibrations. This regular motion might be something like, for example, symmetric or antisymmetric stretching motion of two NO bonds, in which the two bonds vibrate with the same amplitude. At present, we consider that the latter is more probable, because we have found (though not shown here) that the vibrational distribution of path 1 has a non-Boltzmann-type shape peaked at $v=2-3$, which indicates incomplete randomization. For validating either of these two scenarios, it is necessary to further investigate the motion of the direct paths in terms of the geometrical structure of the phase space. Analyses in this direction are now underway.[31]

IV. SUMMARY AND CONCLUSIONS

We have constructed a new PES for the reaction of $O(^1D)+N_2O$, and performed the QCT calculations on the PES. The QCT calculation reproduced semiquantitatively the experimental vibrational distribution,[2,3,10] especially the similar excitation of the two NO products.

It is newly found that the trajectories of this reaction can be classified into four paths, and the extent and mechanism of the vibrational excitation of the "old NO" are different for these paths. In paths 1 and 2, the reaction proceeds through *trans*-type geometry with direct mechanism. The difference of these two is the direction of approach of the $O(^1D)$ atom. In path 1, the reactants approach in collinear geometry, while in path 2 they approach through L-shaped geometry. In spite of the short lifetime, these two paths produce similar excitation of NO and N′O′. In paths 3 and 4, the system passes by the Y-shaped minimum structure. Path 3 has a long lifetime in the Y-shaped well and produces almost equal amount of normal (NO+N′O′) and scrambled (NO′+N′O) products. In spite of the long lifetime, the difference in vibrational energy of the two NO products is relatively large, because most of the exothermicity is released after the barrier. Path 4 exhibits a short lifetime in spite of the deep Y-shaped well, and yields only normal (NO+N′O′) channel products. This path has the largest difference in the distribution of the two NO's. Trajectories belonging to each of these four paths are located at the respective areas in the initial condition space. Note that the regularity in path 4 implies that a deep well does not always ensure chaotic behavior.

The present work is the first recognition of the existence of more than one mechanism for this reaction. Although our calculations are based on the reduced dimension approximation, we expect the real three-dimensional reaction has similar features. In fact, full-dimensional calculations will also exhibit several different paths. However, the full-dimensional calculations, although difficult, would be necessary for full understanding of the dynamics. Furthermore, separate analyses on each of the paths are also inevitable. We have also shown for the first time the existence of the short-lifetime paths (paths 1 and 2) with unexpectedly efficient energy ex-

change, whereas a short-lifetime for this reaction has been only "expected" from the absence of low-energy intermediate. For understanding of the mechanism for this efficient energy transfer, detailed investigation of the phase space structure would be desirable in the future.

[1] R. D. Levine and R. B. Bernstein, *Molecular Reaction Dynamics and Chemical Reactivity* (Oxford University Press, New York, 1987).
[2] H. Akagi, Y. Fujimura, and O. Kajimoto, J. Chem. Soc., Faraday Trans. **94**, 1575 (1998).
[3] H. Akagi, Y. Fujimura, and O. Kajimoto, J. Chem. Phys. **111**, 115 (1999).
[4] K. Honma, Y. Fujimura, O. Kajimoto, and G. Inoue, J. Chem. Phys. **88**, 4739 (1988).
[5] M. Brouard, S. P. Duxon, P. A. Enriquez, R. Sayos, and J. P. Simons, J. Phys. Chem. **95**, 8169 (1991).
[6] M. Brouard, S. P. Duxon, P. A. Enriquez, and J. P. Simons, J. Chem. Phys. **97**, 7414 (1992).
[7] X. Wang, H. Li, Q. Zhu, F. Kong, and H. Yu, J. Chin. Chem. Soc. (Taipei) **42**, 399 (1995).
[8] H. Tsurumaki, Y. Fujimura, and O. Kajimoto, J. Chem. Phys. **111**, 592 (1999).
[9] P. J. Pisano, M. S. Westley, and P. L. Houston, Chem. Phys. Lett. **318**, 385 (2000).
[10] G. Hancock and V. Haverd, Phys. Chem. Chem. Phys. **5**, 2369 (2003).
[11] S. Kawai, Y. Fujimura, O. Kajimoto, and T. Takayanagi, J. Chem. Phys. **120**, 6430 (2004).
[12] J. R. Hetzler, M. P. Casassa, and D. S. King, J. Phys. Chem. **95**, 8086 (1991).
[13] E. A. Wade, J. I. Cline, K. T. Lorenz, C. Hayden, and D. W. Chandler, J. Chem. Phys. **116**, 4755 (2002).
[14] I. Last, A. Aguilar, R. Sayós, M. González, and M. Gilibert, J. Phys. Chem. A **101**, 1206 (1997).
[15] M. González, R. Valero, J. M. Anglada, and R. Sayós, J. Chem. Phys. **115**, 7015 (2001).
[16] H. Akagi, A. Yokoyama, Y. Fujimura, and T. Takayanagi, Chem. Phys. Lett. **324**, 423 (2000).
[17] T. Takayanagi and A. Wada, Chem. Phys. **269**, 37 (2001).
[18] T. Takayanagi and H. Akagi, Chem. Phys. Lett. **363**, 298 (2002).
[19] C. B. Cleveland and J. R. Wiesenfeld, J. Chem. Phys. **96**, 248 (1992).
[20] D. G. Sauder, J. C. Stephenson, D. S. King, and M. P. Casassa, J. Chem. Phys. **97**, 952 (1992).
[21] R. Sayós, C. Oliva, and M. González, J. Chem. Phys. **113**, 6736 (2000).
[22] T. Takayanagi, Chem. Phys. **211**, 308 (2005).
[23] See EPAPS Document No. E-JCPSA6-124-009615 for the detail of the PES function constructed in the present paper. This document can be reached via a direct link in the online article's HTML reference section or via the EPAPS homepage (http://www.aip.org/pubservs/epaps.html).
[24] by H.-J. Werner, P. Knowles, J. Almlöf *et al.*, MOLPRO, a package of *ab initio* programs.
[25] W. Eisfeld and K. Morokuma, J. Chem. Phys. **113**, 5587 (2000).
[26] M. A. Vincent, I. H. Hillier, and L. Salsi, Phys. Chem. Chem. Phys. **2**, 707 (2000).
[27] A. R. W. McKellar, J. K. G. Watson, and B. J. Howard, Mol. Phys. **86**, 273 (1995).
[28] L. Krim and N. Lacome, J. Phys. Chem. A **102**, 2289 (1998).
[29] W. H. Press, S. A. Teukolsky, W. T. Vetterling, and B. P. Flannery, *Numerical Recipes in C* (Cambridge University Press, Cambridge, 1992).
[30] T. Martínez, M. L. Hernández, J. M. Alvariño, F. J. Aoiz, and V. Sáez Rábanos, J. Chem. Phys. **119**, 7871 (2003).
[31] S. Kawai, Y. Fujimura, O. Kajimoto, T. Yamashita, C.-B. Li, T. Komatsuzaki, and M. Toda, J. Chem. Phys. (submitted).